Coral Reefs (2004) 23: 60–73
DOI 10.1007/s00338-003-0354-x

REPORT

J. D. Hedley · P. J. Mumby · K. E. Joyce · S. R. Phinn

Spectral unmixing of coral reef benthos under ideal conditions

Received: 27 February 2003 / Accepted: 6 August 2003 / Published online: 10 December 2003

Abstract Hyperspectral remote sensing has shown promise for detailed discrimination of coral reef substratum types, but, by necessity, it samples at pixel scales larger than reef substratum patch sizes. Spectral unmixing techniques have been successful in resolving subpixel areal cover in terrestrial environments. However, the application of spectral unmixing on coral reefs is fundamentally challenging, due not only to the water column, but also to the potentially large number of spectrally similar and ecologically significant end-member (substratum) classes involved. A controlled ex-situ experiment was conducted using field-spectrometer data to assess the accuracy of spectral unmixing techniques to estimate the areal cover of small-scale (< 0.25 m^2) assemblages of reef substrata (e.g., changes in cover between massive corals, branching corals, bleached corals, macroalgae, and coralline red algae). Mixture compositions were obtained precisely by analysis of digital images collected by a camera calibrated to the field of view of the spectrometer. Linear unmixing techniques were applied to derive estimates of substratum proportions using the full spectral resolution data and various transformations of it, including derivatives and down sampling (merging adjacent wavelengths into broader spectral bands). Comparison of actual and estimated substratum proportions indicate that spectral unmixing may be a practical approach for estimating subpixel-scale cover of coral reef substrata. In the most accurate treatment, coefficients of determination across all mixture sets were high for most end-member classes (37 of 52 cases with $r^2 > 0.64$, i.e. $r > 0.8$). The most successful analyses were based on derivatives of down-sampled data, implying that spectral unmixing benefits more from spectral smoothing and judicious choice of band locations than from high spectral resolution per se. Although these results show that changes in coral and algal cover can be determined by unmixing their spectra, the method is not yet an operational remote sensing tool. Primary empirical research is needed before taking the next step, which is to incorporate a water column, of variable depth, above the sea bed.

Keywords Hyperspectral · Remote sensing · Spectral unmixing

J. D. Hedley (✉) · P. J. Mumby
Marine Spatial Ecology Lab,
School of Biological and Chemical Sciences,
Hatherly Laboratory,
University of Exeter,
Exeter, EX4 4PS, UK
E-mail: j.d.hedley@exeter.ac.uk
Tel.: +44-1392-263784
Fax: +44-1392-263700

K. E. Joyce · S. R. Phinn
Biophysical Remote Sensing Group,
School of Geography,
Planning and Architecture,
University of Queensland,
Brisbane, Queensland,
Australia 4072

Introduction

Coral reefs are threatened by many large-scale processes including rising sea temperature (Hoegh-Guldburg 1999), changes to the biogeochemical properties of sea water (Kleypas et al. 1999), and widespread over-harvesting of resources (Jackson et al. 2001). Monitoring the health of reefs at scales appropriate to these threats is prohibitively expensive by field survey. Satellite or high-altitude airborne sensors provide a more cost-effective platform for observing reefs (Mumby et al. 1999), but routine monitoring of reef health is not yet possible. Measures of reef health that are theoretically amenable to remote sensing include the cover of living, dead, and bleached corals, and functional forms of algae.

Current satellite sensors are incapable of resolving the aforementioned reef substrata principally because of the limited number (< 4) and lack of specificity of spectral bands (Andréfouët et al. 2002; Mumby and Edwards 2002; Hochberg and Atkinson 2003). In

practice, hyperspectral airborne sensors such as the Compact Airborne Spectrographic Imager (CASI; which can record reflectance in 20 or more spectral bands) can resolve several measures of reef "health" (e.g., live coral cover), providing that the water column is shallow (< 10 m) and clear (horizontal Secchi distance > 20 m) and that pixel sizes are around 1 m^2 or less (Mumby et al. 2001). Many (or at least several appropriately placed) spectral bands are needed to discriminate subtleties in spectra between substrata, and small pixels are required to minimize the occurrence of having more than one substratum in a pixel. Conventional "hard" spectral classification schemes are problematic when applied to mixed substratum pixels because each pixel must be assigned to a single substratum category. However, attempting to match the scale of pixels to the patches of reef substrata limits remote sensing in two important ways. First, patches of many substrata are beyond the resolution of existing hyperspectral remote sensing instruments. For example, Andréfouët et al. (2002) concluded that bleached and non-bleached coral colonies would only be distinguishable in pixels of a mere 0.01 m^2. Second, data acquisition would be more cost-effective if substrata could be resolved from larger pixels (and, therefore, larger image extents). Current and planned satellite instruments with hyperspectral capability (e.g., Hyperion, MERIS, MODIS) will retain pixels sizes from 30×30 m to 1×1 km (Townshend and Justice 2002). Thus, the pixel sizes of future satellite sensors will be at least an order of magnitude larger than patches of reef substrata and the problem of mixed pixels is perpetual.

In terrestrial environments, the composition of mixed pixels has been resolved by spectrally unmixing the contribution of each substratum type based on known, pure "end-member" spectra of each substratum (Adams et al. 1986; Foody and Cox 1994). Linear spectral unmixing assumes that the reflectance of a pixel is the sum of the end-member spectra scaled in linear proportion to the cover of each end member within the pixel (Mather 1999; Settle and Drake 1993). However, spectral mixing may not follow this simple linear model due to the morphology of the targets and, in aquatic environments, the presence of the water column and water surface may introduce further complications. Specific approaches to aquatic spectral unmixing are required (e.g., Hedley and Mumby 2003), but thus far very few have been developed.

A fundamental question for reef remote sensing is the extent to which reef substratum cover can be estimated by spectral unmixing in commercially available image data sets. Many living reef components share similar pigments and the spectral separability of non-living components is often confounded by the presence of epilithic algal film or turf (Hedley and Mumby 2002). In this paper, we take the first step in evaluating the efficacy of linear spectral unmixing for coral reefs. The aim was to perform a controlled ex-situ unmixing experiment that avoided complicating factors such as a water column and uncertainty in pixel content. Specifically, we tested the degree to which linear spectral unmixing accurately estimates areal cover of living corals, dead corals, bleached corals, and functional forms of algae (coralline red algae, fleshy phaeophytes, etc.). Two types of spectral data were compared: full, hyperspectral information and discrete spectral bands analogous to those acquired from remote sensing instruments. The experiment was conducted ex situ using field spectrometers, allowing direct control on the cover of each reef substratum, and removing complicating effects of water column, air–water interface, and sensor optics.

Field methods

Data were acquired in two experiments. The larger study was conducted at Palau, Micronesia, in September 2002, and involved investigating the spectral mixing of several groups of end members (later referred to as the "main experiment," ME). A smaller study conducted in March 2002 at Heron Island, Great Barrier Reef (GBR), was specifically concerned with the possibility of unmixing bleached coral cover in conjunction with various other substratum types ("bleaching experiment," BE). The general methodology was the same in both experiments, but the design of the larger study incorporated many more replicates and additional techniques to minimize errors. In addition to the absence of a water column, the main experiment was "idealized" in the sense that the number of end members in each mixture group was restricted to three or four, and only the included end members were applied in the unmixing analysis (in a reef context this would constitute a priori knowledge of the substratum types present). In the bleaching experiment, eight end members were used in total, many of which were only present at all in a few specific mixtures. This latter analysis therefore, more closely represents the application of unmixing without detailed knowledge of which end members are involved.

Substratum samples

In both experiments, small samples of reef substrata (< 15 cm radius) were collected from shallow reef areas and stored in holding tanks for the duration of the experiment (6 days for the ME, 2 h for the BE). Eleven distinct substratum types were used as end members in the main experiment and eight were used in the bleaching experiment (Table 1). In the ME, each substratum type was represented by several actual "pieces" of the material. As a group, these pieces represented a "pool" of material for that end member, from which any specific representation of that end member was drawn at random. Although each "end-member pool" is unlikely to encompass the full natural variation of that substratum type, ecological end members can exhibit quite a high variance in spectral properties even at species level (Hedley and Mumby 2002). This situation should be contrasted with geological remote sensing and unmixing, where mineral end members are relatively spectrally invariant. Therefore, our sampling strategy represents a reasonable first step in applying unmixing to coral reef substrata, given the practical limitations of conducting a controlled experiment.

Fourteen distinct combinations of end members (or "mixture groups") were combined for the mixture measurements. For each mixture group the proportions of the end members were varied over 20–30 replicates and a spectra taken of each (by the method outlined below), giving a total of 296 mixture spectra (Table 2). For each specific mixture set-up, the end-member material consisted of a random selection from the pool of material for that end member. The 14 mixture groups were chosen to represent various realistic scenarios of change in reef communities (see Table 3). These

Table 1 Substratum types used in the bleaching study and main experiment. In later figures and tables substratum types from the main experiment are denoted by the codes indicated

General type	Bleaching experiment	Groupings experiment	
	Specific sample	Code	Specific sample
Live coral	*Montastrea* sp.	M	Columnar *Montipora* sp.
	Pocillopora sp.	Po	Massive *Porites* sp.
		At	*Acropora* sp. (thin branches, < 5 mm)
		Am	*Acropora* sp. (medium branches, 8–15 mm)
Bleached coral	Bleached *Acropora* sp.		
Dead coral	Dead *Pocillopora* sp.	Cr	Coral rubble
Mixed algae		T	Turf algae
Brown algae	*Padina* sp.	Pc	*Padina* sp. (calcified)
	Caulerpa sp.	D	*Dictyota* sp.
Green algae	*Halimeda* sp.	H	*Halimeda* sp.
Red algae		R	Red coralline algae (on rubble)
Sand	Sand	S	Sand

Table 2 Mixture groups from the main experiment. The number of recorded spectra in each group is shown. The spectra within each group represent different arrangements and proportions of the listed end members

Codes	Spectra	Mixture
Am/Cr/S/T	25	*Acropora*, coral rubble, sand, and turf algae
At/D/S	31	*Acropora*, *Dictyota*, and sand
At/H/S	23	*Acropora*, *Halimeda*, and sand
At/Po/S	23	*Acropora*, massive *Porites*, and sand
Cr/H/R/S	24	Coral rubble, *Halimeda*, red coralline algae, and sand
Cr/M/S	20	Coral rubble, columnar *Montipora*, and sand
Cr/Pc/S	20	Coral rubble, calcified *Padina*, and sand
Cr/Po/R/S	20	Coral rubble, massive *Porites*, red coralline algae, and sand
Cr/R/S	20	Coral rubble, red coralline algae, and sand
H/Pc/S	20	*Halimeda*, calcified *Padina*, and sand
H/Po/R/S	10	*Halimeda*, massive *Porites*, red coralline algae, and sand
H/Po/S	20	*Halimeda*, massive *Porites*, and sand
M/Pc/S	20	Columnar *Montipora*, calcified *Padina*, and sand
Pc/Po/S	20	Calcified *Padina*, massive *Porites*, and sand

"change scenarios" were used to provide a meaningful framework for the experiment. However, because this experiment is a first stage in building remote sensing tools for measuring coral cover, we do not imply that detection of such "change scenarios" validates practical application to reef remote sensing.

Note that sand is included as an end member for all mixtures because it comprised the background to the other mixture components. Although in a real reef context sand may not occur so ubiquitously in all circumstances, the experimental method required some kind of background. Sand was considered preferable to the unnatural plastic surface of the tray.

Spectra of substratum mixtures

In each experiment, a selection of samples were placed in a tray with a sand-covered bottom. The tray was filled with just enough water so that the algal samples could assume their natural form and no samples protruded above the water surface. The equipment was sited outdoors close to the collection site. Atmospheric conditions were generally clear with high cirrus for the bleaching experiment, and intermittently clear for the main experiment. Spectral radiance readings of each arrangement of samples were taken using a spectroradiometer with the sensor pointing vertically downwards directed at the center of the scene (Fig. 1). To calculate spectral reflectance, a reference measurement of downwelling irradiance was taken simultaneously with the target spectra (reflectance in both experiments meaning the ratio of radiance to irradiance, in units sr^{-1}). In the main experiment, two GER 1500 spectroradiometers were used to collect the target and reference spectra: the target via a fiber-optic probe from a 3º lens on a horizontal Spectralon panel. The two sensors were electronically synchronized by a data logger. Spectra in the bleaching experiment were collected using an ASD FieldSpec UV/VNIR/CCD and fiber-optic probe for upwelling radiance and a RAMSES ACC with a cosine collector for downwelling irradiance, these sensors were synchronized manually.

In both experiments, a fiber-optic target sensor was deployed with a relatively wide field of view (FOV; ~25° in both cases). In the bleaching experiment, the sensor was mounted 25 cm above the scene giving a sample area of diameter ~11 cm (assuming a circular FOV). In the main experiment, the sensor was mounted at a height of 40 cm, giving a sample area of around 16 cm diameter. By locating the FOV in the scene and ascertaining the coverage of the samples present within it, the exact composition of the sampled mixture could be determined. This scheme assumes that the sensor FOV is circular and of uniform sensitivity across the area of the FOV, and also that the FOV is not in any way wavelength dependent. Imprecise knowledge of the FOV characteristics would seriously compromise the accuracy of the entire experiment by introducing errors or skewing the linearity of the spectral mixing. In practice, spectroradiometer sensors may deviate significantly from a uniform circular model (Rollin and Anderson 2000, cite a 15º lens that was found to have a rectangular FOV of 8×2.5º). A circular uniform FOV was assumed for the BE, but an additional set of data were collected in the ME to characterize the FOV of the sensor and to ensure that none of the above-mentioned factors were a significant source of error. The spectral dependence (in the range 400–700 nm) across the area of the FOV was ascertained by taking readings from different combinations of black and white masks. Results (not shown) confirmed that spectral sensitivity was spatially invariant and that the FOV was circular and constant at all wavelengths. This data also served to locate the position of the FOV in the digital images, and thus it was possible to precisely extract from the digital images the area captured by the FOV. Although these methods and results are not included here for sake of brevity, it should be stressed that a perfect knowledge of the FOV characteristics is required if the experiment is to be duplicated.

End-member spectra

Spectra of the pure end members in the BE were obtained by covering the FOV with one substratum type. However, this was problematic because, in some cases, the samples were too small to

Table 3 Live coral estimation accuracy in the context of various reef "scenarios" (coefficients of determination between actual and estimated substratum proportions for the most successful treatment, derivatives of the resampled spectra). The environment, substrata, and possible change event typified by each mixture group is related to the accuracy of live coral estimation in that situation, under the idealized conditions of this experiment. Values of $r^2 \geq 0.49$ ($r \geq 0.7$) are *emboldened*

Mixture	Potential change scenario	Live coral r^2
Am/Cr/S/T	Mortality event under conditions of high herbivory, e.g., post-bleaching events in *Acropora* spp.-dominated areas	**0.66**
D/At/S	*Acropora* spp. mortality event under conditions of low herbivory leading to dominance of brown macroalgae	**0.81**
H/At/S	*Acropora* spp. mortality event under conditions of low herbivory with green calcareous algal dominance	0.03
M/Cr/S	Further mortality of live corals in areas where mortality has occurred previously in recent years	**0.64**
M/Pc/S	Mortality or recovery of live corals in upper reef slope or lagoonal areas with prolific brown macroalgae	0.39
Pc/Po/S	Changes in cover of long-lived massive *Porites* spp. in areas favored by brown macroalgae (i.e., low herbivory or sheltered environments)	**0.53**
H/Po/S	Changes in cover of long-lived massive *Porites* spp. in areas favored by green calcareous macroalgae	**0.83**
Cr/Po/R/S	Changes in cover of long-lived massive *Porites* spp. in a highly grazed system	**0.77**
H/Po/R/S	Highly grazed system dominated by massive corals (*Porites* spp.), increasing in macroalgae and reducing in red coralline algae (due to herbivory and/or nutrient levels)	**0.87**
At/Po/S	Successional development of reef structure from branching to large massive colonies	*Acropora* **0.91** *Porites* 0.43

cover the FOV. In the ME, end-member spectra were obtained using a 3° lens on the target sensor. Note that using a smaller FOV for the end-member measurements does not compromise the design of the experiment because taking the mean of several such readings is the equivalent of sampling with a larger FOV (see below).

In the BE, the reflectance of each end member or combination of end members was recorded once. Thirty mixes of spectra were taken of which 17 included bleached coral. Replication was extended in the ME with around 20 spectra being taken of each end member, for each reading the target was moved or exchanged for another piece from the pool of material for that end member. The mean of 20 spectra was used in the analysis. These mean spectra, therefore, represent an unbiased estimate of the reflectance of each "end-member pool" as a whole.

Determining actual mixture compositions

A digital image of each arrangement of samples was recorded from directly above the scene, immediately after the spectral signal was recorded by the spectroradiometer. In the BE, images were recorded with a handheld video camera, but this was refined in the ME by using a computer-controlled digital camera mounted on the tripod boom arm next to the spectroradiometer sensor (Fig. 1).

The image of each mixture set-up was loaded into an image-manipulation program, and each end-member type was delineated in a separate color, generating a "template" (Fig. 1). Then, the number of pixels of each type (identified by color) within the FOV was counted by customized program. This program superimposes the FOV on the template image and sums the pixels of each type

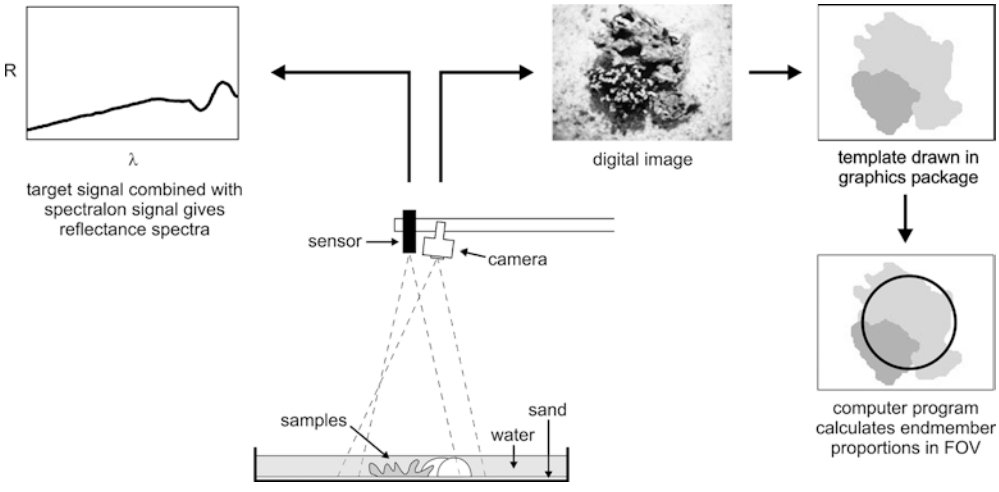

Fig. 1 Apparatus used to simultaneously record reflectance spectra and digital images of mixture set-ups

weighted by the sensitivity of the FOV at that point. In this way, an estimate of the expected proportions of each end member in the spectral signal is attained independently of the characteristics of the sensor hardware. This technique requires that the FOV be fully characterized for spatial sensitivity and also that the FOV be located on the image accurately, as previously discussed.

Analysis techniques

Data processing

Spectra in the BE were collected using the ASD (upwelling radiance) and RAMSES (downwelling irradiance) instruments and were re-sampled to 5-nm intervals to match the RAMSES native resolution. In the ME, data from both GER 1500s were re-sampled to 1-nm intervals. In each measurement scheme, the calculated reflectance is approximately equivalent to "remote sensing reflectance," which is equivalent to the water-leaving signal measured over coral reefs by airborne or satellite imaging systems (the ratio of upwelling radiance to downwelling irradiance, Mobley 1994). The reflectance spectra used in the analysis were restricted to the region 360–740 nm, since longer wavelengths do not penetrate water sufficiently to be of utility in aquatic remote sensing.

Spectral space diagrams

Spectral reflectance data are presented in later sections using a form of diagram that requires some explanation. These "spectral space diagrams" are a useful way to visualize the relationships between end-member spectra and the spectra of their mixtures. A spectral signal recorded in n bands can be thought of as a point in n-dimensional space or "spectral space." The location of the point in each dimension (or axis) is determined by the magnitude of the reflectance in each band. In this view, three end members with dissimilar spectra consist of three points in n-dimensional space. These three points form the corners of a flat triangle that lies in a two-dimensional plane at some orientation in the n-dimensional space (Fig. 2). Any spectral signal that is a "correct" linear mix of the three end-member spectra will lie in the plane of the triangle and within its bounds ("correct" implying that the endmember proportions sum to unity). The end-member triangle can be drawn in two dimensions by rotating the spectral space such that the end-member triangle is brought "flat" into the diagram (Fig. 2) After this, the end-member spectra are described by only two parameters (the x and y positions in the plot). The length of the sides of the end-member triangle in the plot gives an indication of the spectral similarity of the end members; short sides indicate similar spectra.

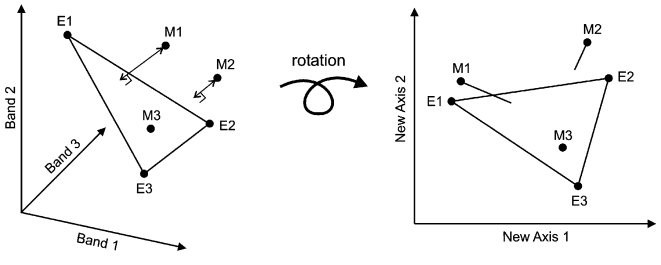

Fig. 2 Generation of "spectral space diagrams." *Left side*: three end members measured in n bands (in this case $n = 3$) form a triangle in n-dimensional spectral space. *Right side*: the space is rotated to bring the end-member triangle into the plane of the diagram. The perpendicular distance of the mixtures from the end-member plane is represented by line segments flattened into the diagram (the line segments are directed to the triangle center; thus, the directions convey no particular meaning)

The mixture spectra can also be plotted onto the end-member triangle by applying the same rotational transform as derived from the end members. This gives an indication where the mixture spectra lie in spectral space in relation to the end-member spectra (an equal mix of all three end members should lie in the center of the triangle, for example). However, in this case, because the mixture spectra may deviate from a perfect linear mix of the end-member spectra, they may lie outside the plane of the end-member triangle (i.e., outside the plane of the paper on which the diagram is drawn). Their location on the two-dimensional plot represents the point in the plane of the triangle that is closest to their actual location. To represent the distance of each mixture spectra from the end-member plane, a line is extended from the location in the two-dimensional plot, the length of which is equal to their distance from the plane. The length of this line gives a visual indication of how close the mixture is to a "correct" linear mix of the end members. This is analogous to "flattening" the perpendicular vector between the end-member plane and the mixture spectrum into the plane of diagram (Fig. 2). Note that, in these diagrams, the line segment is directed toward the center of the triangle for clarity, and the direction itself has no informational meaning.

Therefore, these diagrams become a very useful tool to appreciate the magnitude of deviations from linear mixing in three end-member situations. If mixture spectra are represented by lines that are longer than the distance between two end members, this means the mixture spectra are more different from a "correct" linear mix than the end members are different from each other. If the mixture spectra closely represent linear mixes of the end members, the spectral space plots should consist of very short lines contained within the bounds of the end-member triangle.

Unmixing analysis

Classic least-squares method

Unmixing of the reflectance spectra of the mixtures was achieved using the "classic estimator" least-squares and unconstrained unmixing approach, calculated as follows (Settle and Drake 1993),

$$f = (M^{\mathrm{T}}M)^{-1}M^{\mathrm{T}}x \tag{1}$$

where **M** is the "end-member matrix," an $n \times m$ matrix in which each of m columns is the end member reflectance spectra (measured in n bands), **x** is the measured spectral signal, and **f** is the vector of least-squares estimated end-member proportions. Note that if the end-member spectra are not linearly independent, then the term $(\mathbf{M}^{\mathrm{T}}\mathbf{M})^{-1}$ is not calculable and the system is not solvable (this would occur if one end-member spectra could be represented by summing multiples of one or more of the others).

For the ME, the mixtures in each group (Table 2) were unmixed using only the end members of that group as the columns of **M**. The BE was subjected to two treatments: first, all 30 mixtures were unmixed as a single group using all eight end members as the columns of **M**; second, a subset of 24 of the 30 mixture spectra were unmixed with **M** comprised of the six end-member spectra represented in those mixtures.

Unmixing using derivatives of spectral reflectance curves

In both remote sensing and spectroscopy, derivatives have shown utility in enhancing the usable information in spectral data for various applications (Butler and Hopkins 1970a, 1970b). Derivatives highlight differences in the shape of spectral reflectance signatures of different targets, rather than differences that may be due to variations in illumination conditions (i.e., resulting in a vertical shift on the y-axis). Additionally, many methods for calculating derivatives from spectral data involve an element of data smoothing, which can reduce noise at small wavelength scales (i.e.,

meaningless variation between spectral bands in close proximity). Derivatives have been utilized in other coral-reef, remote-sensing studies (Holden and LeDrew 1998; Mumby et al. 2001; Hochberg et al. 2003).

Derivatives are as applicable to the linear mixing model as are the original reflectance spectra because derivatives adhere to the relation:

$$\frac{d(a+b)}{d\lambda} = \frac{da}{d\lambda} + \frac{db}{d\lambda} \quad (2)$$

which means that, in this context, the derivative of the sum of two or more spectra is equal to the derivatives of the individual spectra summed. In other words, by replacing **M** with the matrix of endmember derivatives and **x** with the derivative of the mixture spectra [in Eq. (2), above], the least-squares analysis is applicable.

First-derivative spectra of mixtures and end members were calculated from the reflectance spectra by the Savitzky–Golay method (Savitzky and Golay 1964; Steinier et al. 1972). The first derivative at each point was estimated as the least squares fit to a window of 11 points in the reflectance data, centered on the point of interest (spectra were treated as cubic or quartic). To accommodate the width of the "convolution window," the resulting derivative spectra have ten fewer bands than the original reflectance spectra. One consequence of taking derivatives is that the overall vertical position of the spectra on the *y*-axis becomes irrelevant (i.e., the constant in $y = f(x) + c$ is removed). Although this may not be strictly analogous to "albedo," it is clear that the overall brightness of an end member will play a significantly lesser role in unmixing when derivatives are applied, as opposed to reflectances. The shape of the spectra will be rather more important. Assessing the results of derivative unmixing, therefore, will give an indication of whether the end-member spectra are being differentiated primarily by their relative brightness or by their spectral shape.

Additionally, the Savitzky–Golay method for calculating derivatives performs an element of smoothing and so reduces noise at the small wavelength scale (i.e., at a scale smaller than the width of the "window," which is 11 bands in this case).

Resampled spectral data

The previous three analyses were applied to the high-spectral-resolution data obtained directly from the spectroradiometers (after calibration and the steps described in the Data processing section above). This yielded 381 bands from the ME data, which is a far higher spectral resolution than is achievable with most of the air- and space-borne sensors commonly used in reef studies (although the new Hyperion satellite approaches this with 220 bands). To relate the unmixing analysis to an achievable CASI spectral resolution (as deployed in other reef remote sensing studies), the endmember and mixture spectra from the ME were down-sampled to ten bands of 10-nm width (Table 4). The original data from the ME is spaced at 1 nm, whereas configurable CASI bands consist of consecutive groups of narrower bands spaced at 1.9 nm, each with FWHM ~2.5 nm. Consequently, the down-sampled bands were simply modeled as the mean over the given wavelength range. Attempting to more precisely model the CASI response from the spectroradiometer data is unlikely to yield a significant benefit in accuracy: the detailed information required would be sensor specific (of both the CASI and the spectroradiometer). The chosen locations of the bands were based both on spectral features of the pigmentation of coral reef organisms (Hedley and Mumby 2002) and on results from previous studies, which have indicated useful spectral regions for discrimination (see Table 4). The classic least-squares unmixing approach was applied to the re-sampled data. Because the Savitzky–Golay method is not appropriate for spectra with a small number of irregularly spaced bands, first derivatives of the re-sampled data were calculated by the finite difference method (i.e., as the difference between adjacent bands, divided by the wavelength distance between them). The unmixing analysis was also applied to these derivatives.

Table 4 Wavelength ranges used to resample the spectroradiometer data to ten simulated CASI bands. Because CASI bands in configurable "imaging mode" are composites of several adjacent bands of ~2.5 nm FWHM, the resampled bands were simply taken as the mean reflectance over the 10-nm range. The reason for the position of each band is shown together with the source for that information

Wavelengths (nm)	Notes	Source
430–439	Chl-*a* absorption maxima	Jeffrey et al. (1997)
440–449	Coral fluorescence /Chl-*c*absorption maxima	Dove et al. (2001); Jeffrey et al. (1997)
450–459	Chl-*b* absorption maxima	Jeffrey et al. (1997)
470–479	Peridinin absorption maxima	Jeffrey et al. (1997)
530–539	Previous study	Clark et al. (2000)
570–579	Phycoerythrin absorption maxima	Govindjee and Braun (1974)
620–630	Coral fluorescence	Dove et al. (2001)
640–649	Chl-*b* absorption maxima	Jeffrey et al. (1997)
660–669	Chl-*a* absorption maxima	Jeffrey et al. (1997)
680–689	Previous study	Rundquist et al. (1996)

Assessing unmixing accuracy

Due to the multivariate but non-independent nature of estimated endmember proportions, it is difficult to find an appropriate measure for describing the accuracy of unmixing results. Most of the techniques used to assess accuracy in "hard" classification schemes (such as the Kappa and Tau coefficients; Ma and Redmond 1995) are based on the values from an error matrix (Foody 2002). Because there is no way to cross reference inaccurately identified categories within a single unmixed spectral signal, it is not possible to construct an error matrix for unmixing results, and these measures are not applicable. Additionally, discrete multivariate techniques are used for assessing "hard" classifications, whereas unmixing results are not discrete.

In this study, the accuracy of the estimated proportions has been assessed by performing linear regression between the actual proportion and the estimated proportion for each end member within each mixture combination (i.e., typically 20 replicates). The coefficient of determination of this regression gives the amount of variation in each end member that is explained by the unmixing results. A similar approach utilizing correlation coefficients has been used in previous unmixing work (Foody and Cox 1994), but coefficient of determination was preferred here because it has a tangible meaning, giving a sense of the power of the unmixing analysis. An additional advantage of assessing accuracy by regression is that the approach is equally applicable if the unmixed proportions are "well formed" or not (i.e., take values between zero and one and sum to unity). In order to give an indication of the overall accuracy for each mixture group, the mean coefficient of determination for all of the end members involved was also calculated.

Although specific techniques do exist for assessing non-discrete classification accuracy (Matsakis et al. 2000; Foody 2002), linear regression was chosen here because it is readily interpretable and can be applied to each end member independently.

Results

Spectral data

Figure 3 shows the mean end-member reflectance spectra and a single example mixture reflectance spectrum for four of the mixture groups in the main experiment.

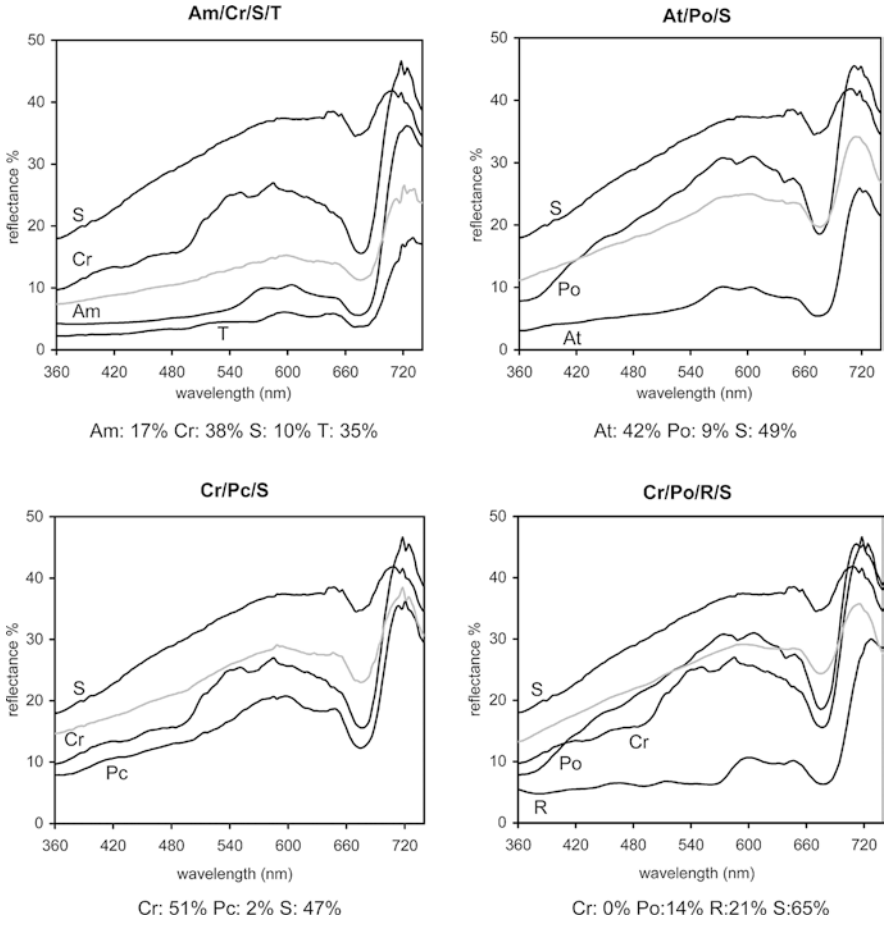

Fig. 3 Mean end-member reflectance spectra and a single-mixture spectrum from four of the mixture groups in the main experiment. The end-member spectra are labeled. The *gray line* is the recorded reflectance from a single-mixture set-up, with end-member cover in the quantities listed

The actual percentage cover of each end member present when the mixture spectra were recorded are also shown. Qualitatively, the mixture spectra appear, as would be expected, from a linear mix of the end-member spectra in the proportions given. Figure 4 gives a more precise indication of how closely the spectral data from the main experiment follow a linear mixing model. The diagrams indicate that in most cases the spectra of the three end members are sufficiently different from each other to form a sound basis for spectral unmixing. Two exceptions, which have the narrowest end-member triangles, suggest that the brown *Acropora* (At) and *Dictyota* (D) samples were spectrally similar relative to sand (S), and that calcified *Padina* (Pc) was quite similar to a mixture between *Montipora* (M) and sand (S). The locations of the mixture spectra in these diagrams (isolated line segments) indicate that in many cases the mixture spectra deviated substantially from a linear mix of end-member spectra. In all ten plots, the mixtures lie at least some distance from the end-member plane. In seven of the ten plots, for the majority of mixtures, the closest point in the end-member plane to the mixtures is outside the end-member triangle. Thus, the majority of mixture spectra did not represent linear mixes of the end-member spectra. In the worst cases (H/Po/S: *Halimeda*, *Porites*, and sand; Cr/M/S: coral rubble, *Montipora*, and sand) the distance of the mixture spectra from the end-member triangle approached the distance between the end members themselves.

The results of re-sampling the spectra to ten bands of 10 nm (Table 4) and taking first derivatives are revealed in Fig. 5. Qualitatively, the results for end members were similar to those from full spectra (Fig. 4) in that At/D/S and M/Pc/S had the narrowest triangles and that the ''openness'' of end-member triangles were similar. A collapse of any of the triangles would indicate that the choice of bands had omitted important spectral information for end-member discrimination. Most strikingly, however, the derivatives of the re-sampled mixture spectra are much improved in terms of their adherence to the linear mixture model. Compared with Fig. 4, in most cases, the mixture spectra lie relatively close to the end-member plane and within the end-member triangle. Thus, re-sampling and taking derivatives transformed the spectra such that they were more closely represented by the linear mixing model.

Main experiment unmixing results

The results from all end-member groups and unmixing methods are presented in Table 5 for the ME. Results from the classical unconstrained unmixing method are reasonably successful if the measure of an ''accurate

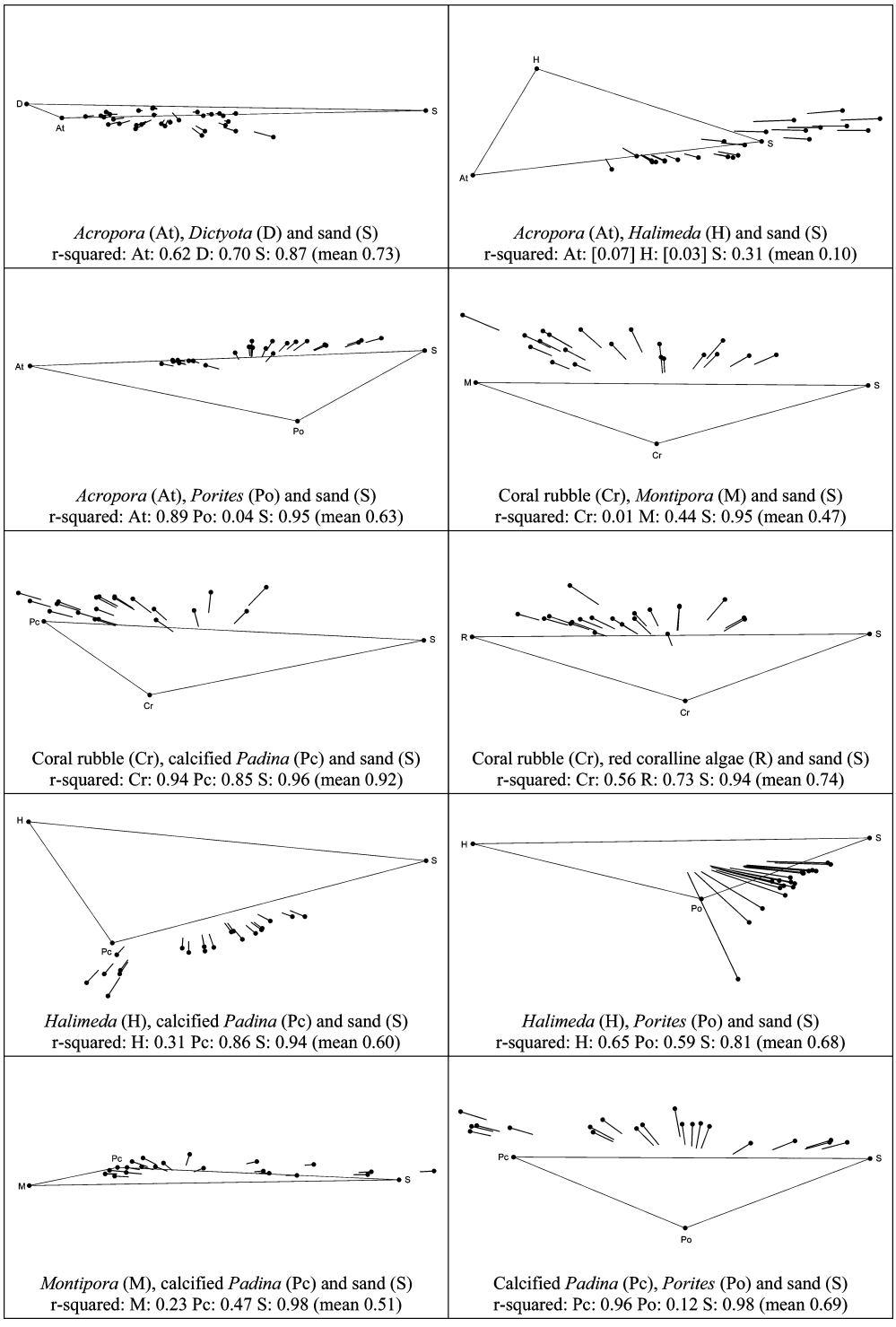

Fig. 4 Spectral space diagrams based on the full spectral resolution reflectance spectra for all three-way mixtures in the main experiment. *Black dots* indicate the relative locations of measured spectral signals in spectral space. The signals from the three end members in each case are labeled and the *triangle* that delimits their 'legitimate' linear mixes is drawn. Line segments represent mixtures: the *inner (pointed) end* is the closest point in the end-member plane to the mixture; the *line length* is the distance of the mixture reflectance from the end-member plane (the direction of the line segments have no meaning; they are orientated to the *triangle center* for clarity)

result'' used by Foody and Cox (1994) is used as a benchmark; namely, a correlation coefficient greater than 0.7 ($r^2 > 0.49$). By this measure, 11 of the 14 mixture groups were unmixed accurately using reflectance spectra (i.e., the mean r^2 over all end members involved is > 0.49). Looking at the individual end-member results within the mixtures, 29 of the total 46 individual r^2 values across all mixture groups are greater than 0.49. First derivatives of the high spectral resolution data improved performance of the classical estimator in 17 of the 46 individual end-member results (Table 5), but impaired performance in 22 cases. A paired sample *t*-test for differences between the treatments (performed on the *r* values transformed by the Fisher transform, Zar 1998) was not significant ($p = 0.48$). Despite this, it is clear from Table 5 that taking derivatives has had a large effect on the unmixing accuracy of individual end members in some isolated cases.

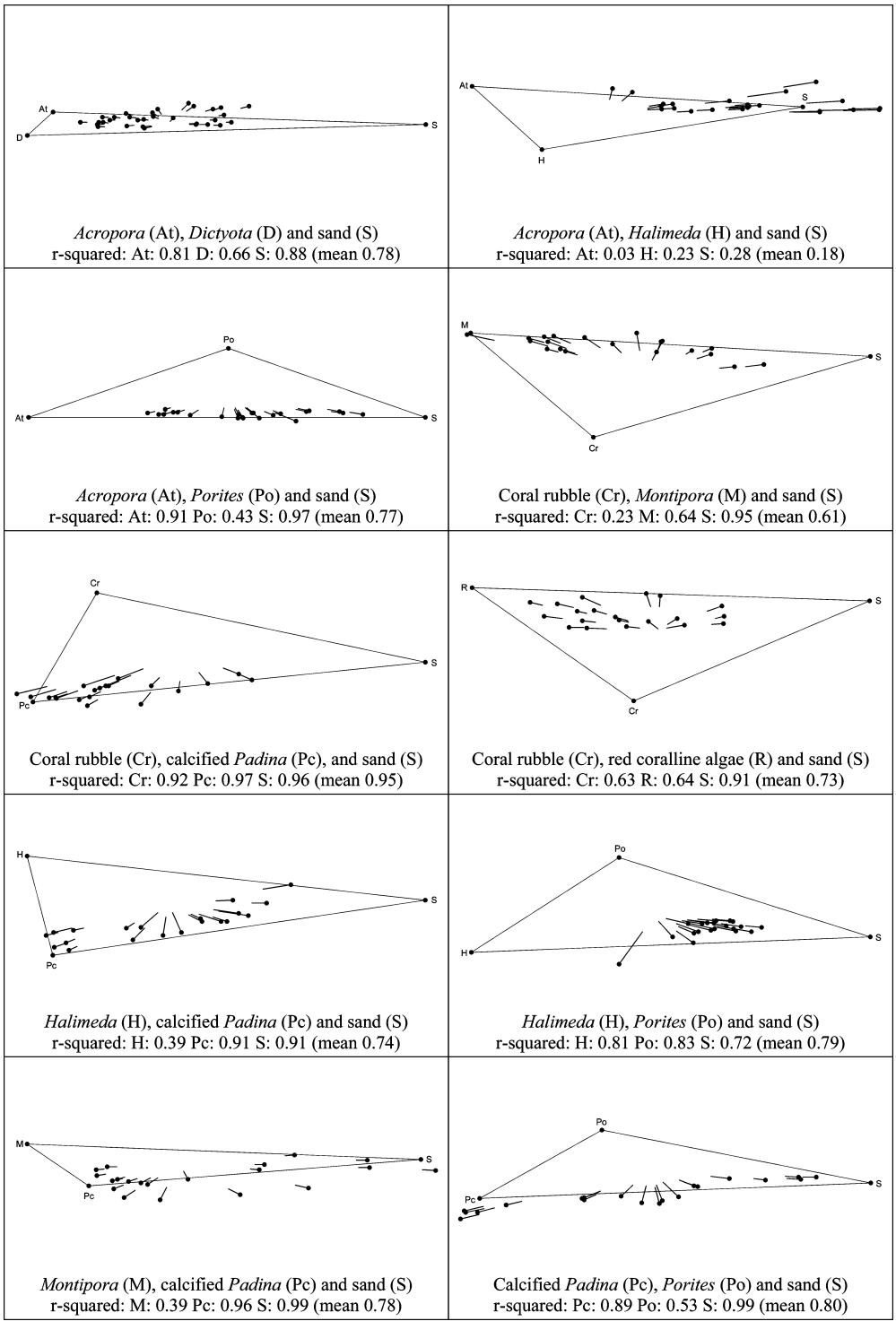

Fig. 5 Spectral space diagrams of mixtures and end members based on derivatives of ten-band re-sampled spectra

The most accurate results overall were from the unmixing of ten-band re-sampled data that had been transformed to first derivatives. In this treatment, 12 of the 14 mixture groups had greater mean r^2 than for linear unmixing applied to the original high spectral resolution reflectances, and in the two exceptions, the mean r^2 only decreased by 0.01 (Table 5). A paired sample t-test for difference in transformed r for individual endmembers between the treatments gave $p < 0.001$. Additionally, in contrast to the full spectra (above), taking derivatives from ten-band spectra had a significant positive impact on the results (again, $p < 0.001$). In fact, for all of the 14 mixture groups, mean r^2 increased under the derivative treatment.

Table 6 shows the mean r^2, and corresponding correlation coefficients, for different end-member categories averaged over all the mixture groups, for the re-sampled derivative treatment. In all but one case, the

Table 5 Results from the main experiment showing coefficient of determinations (r^2) of the regression of estimated proportion against actual proportion for each end member, within each mixture group. Mean coefficient of determination across all end members is calculated for each mixture group. *Figures in square brackets* indicate negative correlations and are treated as zero for the calculation of the mean. Four treatments of the spectral data are shown: the original high spectral resolution reflectance; Savitzky–Golay derivatives; resampled 10-band reflectance; and finite-difference derivatives of the 10-band data. *Emboldened figures* show the best result for each mixture group

	Number	Linear unmixing result (Coeff. of determination)					Re-sampled (Coeff. of determination)				
Am/Cr/S/T		Am	Cr	S	T	Mean	Am	Cr	S	T	Mean
Reflectance	25	0.67	0.27	0.73	0.35	0.51	0.57	0.76	0.72	0.11	0.54
Derivatives	25	0.57	0.02	0.72	0.17	0.37	0.66	0.69	0.73	0.50	**0.65**
At/D/S		At	D	S			At	D	S		
Reflectance	31	0.62	0.70	0.87		**0.79**	0.74	0.22	0.88		0.61
Derivatives	31	0.78	0.66	0.87		0.77	0.81	0.66	0.88		0.78
At/H/S		At	H	S			At	H	S		
Reflectance	23	(0.07)	(0.03)	0.31		0.10	0.01	0.27	0.20		0.16
Derivatives	23	0.25	(0.47)	0.96		**0.40**	0.03	0.23	0.28		0.18
At/Po/S		At	Po	S			At	Po	S		
Reflectance	23	0.89	0.04	0.95		0.63	0.85	0.05	0.97		0.63
Derivatives	23	0.94	0.47	0.95		**0.79**	0.91	0.43	0.97		0.77
Cr/H/R/S		Cr	H	R	S		Cr	H	R	S	
Reflectance	24	(0.42)	0.13	0.91	0.92	0.49	(0.55)	0.11	0.92	0.95	0.50
Derivatives	24	0.16	0.15	0.88	0.92	0.53	(0.32)	0.68	0.93	0.94	**0.64**
Cr/M/S		Cr	M	S			Cr	M	S		
Reflectance	20	0.01	0.44	0.95		0.47	0.09	0.34	0.95		0.46
Derivatives	20	0.00	0.52	0.94		0.49	0.23	0.64	0.95		**0.61**
Cr/Pc/S		Cr	Pc	S			Cr	Pc	S		
Reflectance	20	0.94	0.85	0.96		0.90	0.88	0.98	0.97		0.94
Derivatives	20	0.06	0.67	0.77		0.50	0.92	0.97	0.96		**0.95**
Cr/Po/R/S		Cr	Po	R	S		Cr	Po	R	S	
Reflectance	20	0.13	0.31	0.91	0.95	0.58	0.32	0.42	0.93	0.96	0.66
Derivatives	20	(0.02)	0.63	0.95	0.96	0.64	0.12	0.77	0.94	0.96	**0.70**
Cr/R/S		Cr	R	S			Cr	R	S		
Reflectance	20	0.56	0.73	0.94		**0.74**	0.62	0.64	0.91		0.72
Derivatives	20	0.28	0.61	0.78		0.56	0.63	0.64	0.91		0.73
H/Pc/S		H	Pc	S			H	Pc	S		
Reflectance	20	0.31	0.86	0.94		0.60	0.14	0.91	0.91		0.65
Derivatives	20	0.41	0.93	0.94		**0.76**	0.39	0.91	0.91		0.74
H/Po/R/S		H	Po	R	S		H	Po	R	S	
Reflectance	10	0.52	0.28	0.92	0.88	0.65	0.05	0.25	0.71	0.87	0.47
Derivatives	10	0.26	0.79	0.92	0.92	0.72	0.79	0.87	0.88	0.89	**0.86**
H/Po/S		H	Po	S			H	Po	S		
Reflectance	20	0.65	0.59	0.81		0.68	0.34	0.59	0.72		0.55
Derivatives	20	(0.05)	0.42	0.83		0.41	0.81	0.83	0.72		**0.79**
M/Pc/S		M	Pc	S			M	Pc	S		
Reflectance	20	0.23	0.47	0.98		0.56	0.00	0.42	0.98		0.47
Derivatives	20	0.03	0.63	0.89		0.52	0.39	0.96	0.99		**0.78**
Pc/Po/S		Pc	Po	S			Pc	Po	S		
Reflectance	20	0.96	0.12	0.98		0.69	0.92	0.14	0.99		0.68
Derivatives	20	0.96	0.08	0.97		0.67	0.89	0.53	0.99		**0.80**

Table 6 Results from the main experiment averaged over all mixture sets for end-member type, for the overall best treatment (re-sampled, derivatives). The number of mixture sets from which the mean is calculated is also given

Type	Codes	No. mixture sets	Mean r^2	r
Sand	S	(14)	0.85	0.92
Live coral	At/Am/Po/M	(9)	0.69	0.83
Coral rubble	Cr	(6)	0.43	0.66
Halimeda	H	(5)	0.58	0.76
Red coralline	R	(4)	0.85	0.92
Calcified *Padina*	Pc	(4)	0.93	0.97
Turf algae	T	(1)	0.50	0.71

correlation coefficients are in excess of Foody and Cox's (1994) accepted accuracy level of 0.7.

Bleaching experiment unmixing results

The results from the BE (Tables 7 and 8) followed a slightly different pattern to those from the main experiment. In the full eight end-member unmixing analyses (on 30 mixtures), re-sampling the data to ten bands did not produce a clear improvement. Further, utilizing derivatives had a clearer positive effect on original reflectance data, and little effect on the re-sampled data.

Table 7 Coefficients of determination between unmixed and actual substratum proportions from the bleaching experiment, with the entire dataset (30 mixture spectra) treated as a single eight-end-member group. The highest value of r^2 for each substratum type is *emboldened*

End member	Classical		Re-sampled	
	Reflec.	Deriv.	Reflec.	Deriv.
Sand	**0.21**	0.20	0.15	0.15
Uncalcified *Padina*	0.26	**0.51**	0.11	0.15
Caulerpa	0.19	**0.55**	0.25	0.20
Bleached *Acropora*	0.54	0.71	0.80	**0.81**
Halimeda	0.07	0.17	0.00	0.00
Montastrea	0.39	**0.59**	0.09	0.09
Live *Pocillopora*	0.41	**0.67**	0.59	0.58
Dead *Pocillopora*	0.31	**0.72**	0.10	0.15
Mean	0.30	**0.51**	0.26	0.27

Table 8 Coefficients of determination between unmixed and actual substratum proportions from the bleaching experiment, utilizing a subset of the dataset (24 mixture spectra) treated as a single six-end-member group. The highest value of r^2 for each substratum type is *emboldened*

End member	Classical		Re-sampled	
	Reflec.	Deriv.	Reflec.	Deriv.
Sand	0.29	0.29	0.20	0.20
Uncalcified *Padina*	0.47	0.52	**0.60**	0.53
Caulerpa	0.75	**0.79**	0.68	0.65
Bleached *Acropora*	0.56	0.78	0.78	**0.86**
Live *Pocillopora*	0.38	0.57	0.51	**0.65**
Dead *Pocillopora*	0.50	**0.73**	0.71	0.67
Mean	0.49	**0.61**	0.58	0.59

Attempting eight end-member unmixing is ambitious even for terrestrial applications, and so the analysis was repeated on a subset of data from the same experiment that excluded all mixtures involving *Halimeda* or *Montastrea* (which were the least represented substrata in the data set). The results for this six end-member unmixing (on 24 mixtures) were generally very much better than when the unmixing was attempted with all eight end members (Tables 7 and 8). Therefore, as expected, restricting the number of end members involved increases in unmixing accuracy.

In both cases (Tables 7 and 8), it is interesting to note that while the proportion of some end members may be predicted very poorly, the proportion of others may be estimated very accurately in same analysis. Figure 6 shows scatter plots for the estimation of proportions of live *Pocillopora*, dead *Pocillopora*, and bleached *Acropora* versus actual proportion, based on derivatives of the original data.

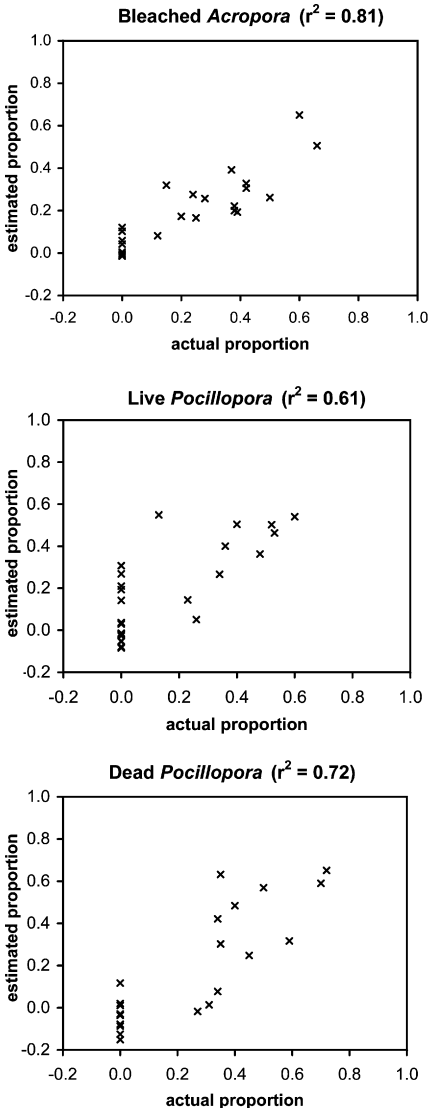

Fig. 6 Scatterplots between actual and estimated proportions for three end members from the bleaching experiment. Unmixing was performed using first derivatives. The analysis represents 24 mixture spectra with a total of six end members

Discussion and conclusions

Technical aspects

Untransformed reef reflectance spectra did not adhere to the linear mixing model. The pattern of clustering in mixture spectra (Fig. 4) suggested that mixtures were the result of some continuous variation between two or more extreme endpoints (i.e., in many cases, the mixtures lie approximately along a line). This kind of pattern would be expected if the mixtures were linear mixes of a set of end members, in which case, the end members should be located at the extreme points of the mixture distributions. However, in most cases, the group of mixture spectra were shifted relative to the actual end-member triangle area, suggesting a systematic error or function. It is possible that the slight differences in methodology used to record the end-member and mixture spectra could have resulted in some inconsistency in the data. However, it is not clear how such errors would arise: the methods are analogous, and target and reference sensors were calibrated at several points throughout the experiment using a Spectralon panel. In

particular, the plots involving *Halimeda* (the only case where end-member spectra were taken from a previous study, but by the same methodology) exhibited some of greatest deviations from the linear mixing model. This may imply that the transferability of spectra across studies is poor because of inter- or intra-specific variation or subtleties in methods. Unmixing results for *Halimeda* were improved by taking derivatives, which may have removed much of the variation in spectra due to ''brightness.'' Indeed, use of derivatives could mitigate some of the problems involved in transferring spectra across studies.

Measurement errors aside, it is quite feasible that spectral mixing among reef substrata is non-linear. Given the controlled nature of the experiment, the differing morphology of samples would seem to be the only cause of non-linear mixing. The spectral reflectance of corals differs significantly with viewing angle, largely because of the geometry of coral colonies (Joyce and Phinn 2002). Therefore, coral reflectance is not controlled solely by the areal extent of a substratum type. Figure 7 shows the mean deviation between the estimated and actual proportions for each end member from each group in the main experiment. It is quite

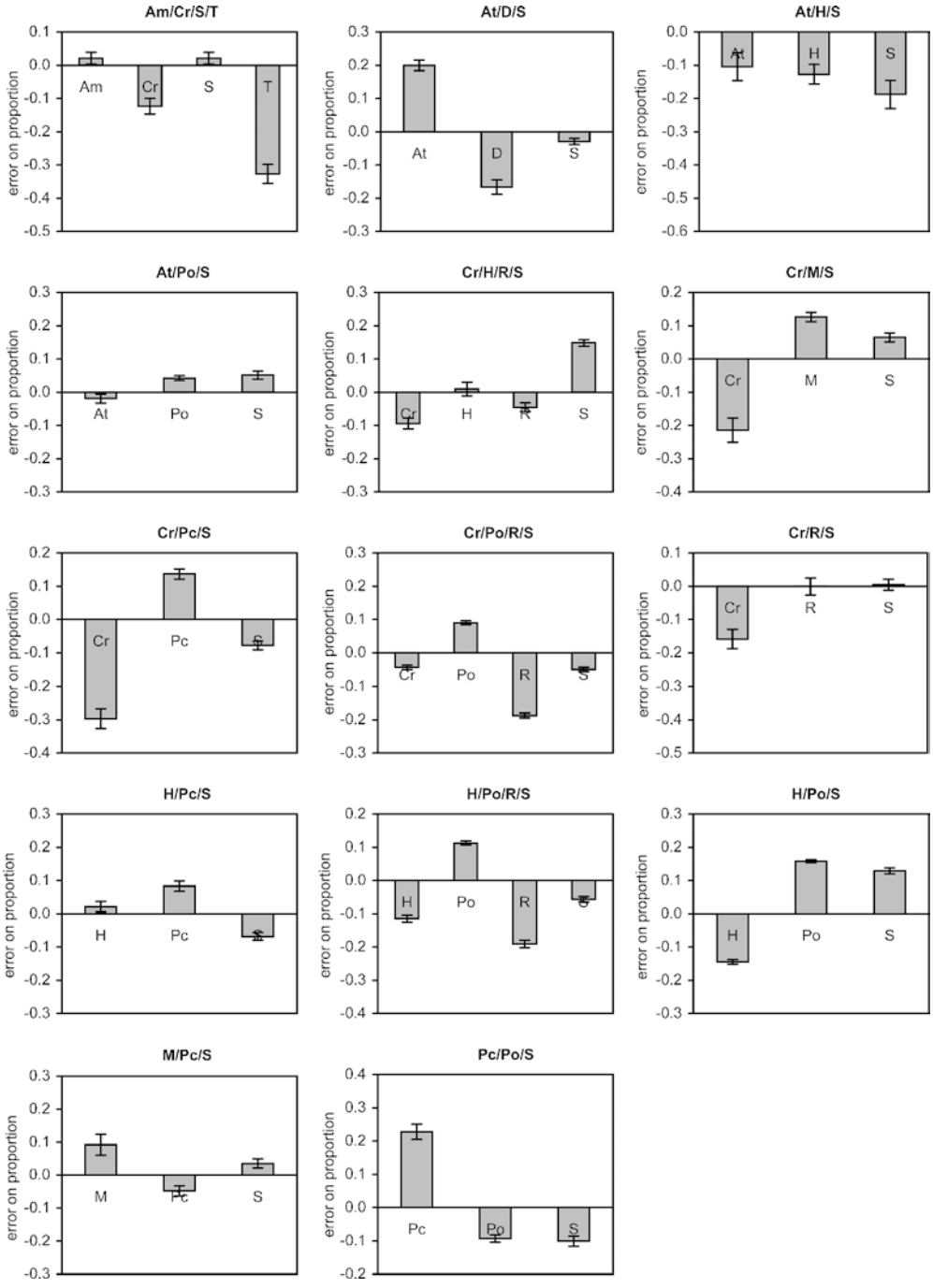

Fig. 7 Mean deviation between actual and estimated proportion for each mixture group, based on the classical unconstrained linear unmixing estimator applied to derivatives of the re-sampled data. *Error bars* represent plus and minus one standard error

striking that, in almost all cases, end members were consistently over-estimated or under-estimated within each mixture group. However, there is little consistency in estimation errors across mixture groups. Sand, for example, is sometimes over-estimated and sometimes under-estimated. It is possible to conjecture a hypothesis that certain end members, in conjunction with certain others, could lead to particular non-linear effects. For example, a "raised" end member such as a coral might tint the appearance of the highly reflective sand surrounding it by light reflecting from its sides. The proportion of the raised end member would then be overestimated and the cover of sand underestimated. It is difficult to discern a clear pattern in the data (Fig. 7) to support such a hypothesis, but this is an important issue for future work because such effects could conceivably have impacts at remote sensing scales (i.e., >1 m^2).

Re-sampling spectral data to fewer, broader spectral bands has a positive effect on the accuracy of unmixing. Spectral data in the BE were re-sampled to 5-nm band widths before analysis, and no subsequent improvement was gained by re-sampling again to 10 nm. Accuracies resulting from the BE were comparable to those from the ME after re-sampling. The ability to distinguish spectra from an appropriate selection of bands has great practical implications because it avoids the complexity of engineering a remote sensing instrument with extremely high spectral resolution. However, there is of course a trade-off because reducing the number of bands reduces the dimensionality of the data and, at the limit, will prevent the spectral separability of substrata (see also Hochberg and Atkinson 2003). As an absolute minimum, having at least as many bands as end members is a mathematical requirement of the classic least-squares unmixing estimator.

Departures from non-linear spectral mixing were reduced by taking first derivatives from re-sampled spectra. Taking finite-difference derivatives removes any constant y-axis shift, but does not additionally smooth the data. The implication is that the position of the reflectance spectra on the y-axis acted to confound the unmixing analysis. Inconsistency between the measurements taken by the target and reference sensors could have caused noise-like deviations, which were predominately reflected the vertical position of the spectra. For example, even though the two sensors in the ME were electronically synchronized, their different integration times may have allowed brief atmospheric changes to bias reflectance spectra, resulting in either over- or under-estimates of albedo.

The mixtures in the ME were also analyzed using second derivatives of the full spectral resolution data to determine if higher derivatives conferred any additional advantage (results not shown). The second derivatives were also calculated by the Savitzky–Golay method with a "convolution window" of 11 bands (assuming a quartic function and using values from Steinier et al. 1972). In all cases, the unmixing accuracy was substantially impaired when based on these second derivatives, and a paired sample t-test for differences between the first derivative and second derivative treatment (performed on the r values transformed by the Fisher transform, Zar 1998) was highly significant ($p < 0.001$). Therefore, for this method of calculating derivatives, utilizing derivatives higher than the first derivative was not advantageous for unmixing analyses.

Reef context

In general, under the most successful treatment (derivatives of the re-sampled data), coral cover was measurable under a variety of ecological scenarios (listed in Table 3). Of the 11 examples of live coral estimation, seven of the r^2 values are greater or equal to 0.64 (i.e., $r \geq 0.8$). In four cases, linear unmixing was able to recover at least 81% of the variation in the live coral proportions (i.e., $r \geq 0.9$).

Porites sp. estimation performed generally well in most contexts tested, but was weakest when the *Porites* sample was combined with the brown macroalgae or *Acropora*. Presumably, the relative spectral similarity of the *Porites* (which was a light brown morph in this case) and the calcified *Padina* had a negative impact on their ability to be unmixed. Estimates of the cover of *Montipora* sp. were weak ($r^2 = 0.39$) when in conjunction with calcified *Padina*. Changes to branching coral cover (*Acropora*), such as those arising from a mass bleaching event, were also resolvable with one exception: *Halimeda* and *Acropora* could not be distinguished effectively, although this may partly be due to problems incurred in gaining an end-member spectra for *Halimeda* (above).

In the BE, the estimation of bleached *Acropora* proportions was consistently accurate under various treatments. This result is promising, first because it is highly desirable to monitor the severity of bleaching, and second, because previous studies found that non-spectral-unmixing approaches are inappropriate for detecting coral bleaching (Andréfouët et al. 2002). Our results suggest that spectral unmixing may offer a realistic solution to monitoring coral bleaching in future.

In this controlled experiment, it has been possible to achieve a reasonable level of accuracy in the estimation of some end-member proportions in analysis of six-way or even eight-way mixes. In practice, unmixing of more than three or four end members would be ambitious, even for a terrestrial study. For some applications, however, it may be acceptable to achieve a poor result for the estimation of most end members providing that the critical substrata were resolved accurately. A good example would be measurement of bleached versus live coral where the cover of algae was not directly relevant to the question of bleaching severity.

In summary, we have demonstrated that, in the absence of the overlying water column and atmospheric attenuation effects, linear spectral unmixing can be of use in determining the proportions of various reef

substrata within a single mixed spectrum. There is evidence for non-linear processes in spectral mixing, but these effects can be mitigated by re-sampling hyperspectral data to lower spectral resolution and by utilizing first derivatives. Our ability to determine the proportion of individual substrata under this best-case scenario is also affected by the number and type of reef components involved. Pending further testing to include atmospheric and water column attenuation parameters, we propose that linear unmixing techniques will be invaluable for use with high spectral resolution data from both airborne and satellite platforms (and possibly, from multispectral sensors optimized for coral reefs), and will provide a more sensitive and accurate representation of reef composition than standard per-pixel, single-substratum thematic classifications. More sophisticated non-linear unmixing methods (as yet undeveloped) may be required to fully exploit the potential in high spectral resolution data from coral reefs.

Acknowledgements This study was funded by the Royal Society and Natural Environment Research Council (UK). We thank the NERC field spectroscopy pool for supplying the spectroradiometers used in Palau. The Heron Island experiment was conducted during the World Bank/GEF/UNESCO/IOC Coral Bleaching Workshop. We thank the staff of the Palau International Coral Reef Center for their kind hospitality and support.

References

Adams JB, Smith MO, Johnson PE (1986) Spectral mixture modelling: a new analysis of rock and soil types at the Viking Lander I site. J Geophys Res 91:8098–8112

Andréfouët S, Berkelmans R, Odriozola L, Done T, Oliver J, Muller-Karger F (2002) Choosing the appropriate spatial resolution for monitoring coral bleaching events using remote sensing. Coral Reefs 21:147–154

Butler RW, Hopkins DW (1970a) Higher derivative analysis of complex absorption spectra. Photochem Photobiol 12:439–450

Butler RW, Hopkins DW (1970b) An analysis of fourth derivative spectra. Photochem Photobiol 12:451–456

Clark CD, Mumby PJ, Chisholm J, Jaubert J, Andréfouët S (2000) Spectral discrimination of coral mortality states following a severe bleaching event. Int J Remote Sensing 21:2321–2327

Dove SG, Hoegh-Guldberg O, Ranganathan S (2001) Major colour patterns of reef-building corals are due to a family of GFP-like proteins. Coral Reefs 19:197–204

Foody GM (2002) Status of land cover classification accuracy assessment. Remote Sensing Environ 80:185–201

Foody GM, Cox DP (1994) Sub-pixel land cover composition estimation using a linear mixture model and fuzzy membership functions. Int J Remote Sensing 15:619–631

Govindjee, Braun BZ (1974) Light absorption, emission and photosynthesis. In: Stewart WDP (ed) Algal physiology and biochemistry. Blackwell, Oxford, pp 346–390

Hedley JD, Mumby PJ (2002) Biological and remote sensing perspectives of pigmentation in coral reef organisms. Advance Mar Biol 43:277–317

Hedley JD, Mumby PJ (2003) A remote sensing method for resolving depth and subpixel composition of aquatic benthos. Limnol Oceanogr 48:480–488

Hochberg EJ, Atkinson MJ (2003) Capabilities of remote sensors to classify coral, algae, and sand as pure and mixed spectra. Remote Sensing Environ 85:174–189

Hochberg EJ, Atkinson MJ, Andréfouët S (2003) Spectral reflectance of coral reef bottom-types worldwide and implications for coral reef remote sensing. Remote Sensing Environ 85:159–173

Hoegh-Guldberg O (1999) Climate change, coral bleaching and the future of the worlds coral reefs. Mar Freshwater Res 50:839–866

Holden HM, LeDrew EF (1998) Spectral discrimination of healthy and non-healthy corals based on cluster analysis, principal components analysis, and derivative spectroscopy. Remote Sensing Environ 65:217–224

Jackson JBC et al. (2001) Historical over fishing and the recent collapse of coastal ecosystems. Science 293:629–638

Jeffrey SW, Mantoura RFC, Bjørnland T (1997) Data for the identification of 47 key phytoplankton pigments. In: Jeffrey SW, Mantoura RFC, Wright SW (eds) Phytoplankton pigments in oceanography: guidelines to modern methods. UNESCO, Paris, pp 449–559

Joyce K, Phinn S (2002) Bi-directional reflectance of corals. Int J Remote Sensing 23(2):389–394

Kleypas JA, Buddemeier RW, Archer D, Gattuso JP, Langdon C, Opdyke BN (1999) Geochemical consequences of increased atmospheric carbon dioxide on coral reefs. Science 284:118–120

Ma Z, Redmond RL (1995) Tau coefficients for accuracy assessment of classification of remote sensing data. Photogramm Eng Remote Sensing 61:435–439

Mather PM (1999) Computer processing of remotely-sensed images, 2nd edn. Wiley, New York

Matsakis P, Andréfouët S, Capolsini P (2000) Evaluation of fuzzy partitions. Remote Sensing Environ 74:515–532

Mobley CD (1994) Light and water. Academic Press, San Diego

Mumby PJ, Green EP, Edwards AJ, Clark CD (1999) The cost-effectiveness of remote sensing for tropical coastal resources assessment and management. J Environ Manage 55:157–166

Mumby PJ, Edwards AJ (2002) Mapping marine environments with IKONOS imagery: enhanced spatial resolution can deliver greater thematic accuracy. Remote Sensing Environ 82:248–257

Mumby PJ, Chisholm JRM, Clark CD, Hedley JD, Jaubert J. (2001) A bird's-eye view of the health of coral reefs. Nature 413:36

Rollin EM, Anderson K (2000) Summary report of laboratory calibrations of GER1500_2 #2038/#2039 in October 2000, NERC EPFS Report Number SR/00/01, NERC EPFS 2000

Rundquist DC, Han L, Schalles JF, Peake JS (1996) Remote measurement of algal chlorophyll in surface waters: the case for the first derivative of reflectance near 690 nm. Photogramm Eng Remote Sensing 62:195–200

Savitzky A, Golay MJE (1964) Smoothing and differentiation of data by simplified least squares procedures. Analyt Chem 36:1627–1639

Settle JJ, Drake NA (1993) Linear mixing and the estimation of ground cover proportions. Int J Remote Sensing 14:1159–1177

Steinier J, Termonia Y, Deltour J (1972) Comments on smoothing and differentiation of data by simplified least square procedure. Analyt Chem 44:1906–1909

Townshend JRG, Justice CO (2002) Towards operational monitoring of terrestrial systems by moderate-resolution remote sensing. Remote Sensing Environ 83:351–359

Zar JH (1998) Biostatistical analysis, 4th edn. Prentice Hall, New Jersey